CHAPTER 3

EXPERIMENTAL AND ANALYTICAL TECHNIQUES

In this chapter, setup for the home-built dual mode plasma assisted hot-wire CVD is presented. Substrates and catalysts used for the SiNWs deposition are described. The modified dual mode system can be altered easily to PECVD, HWCVD or both techniques could be combined subject to the required deposition technique. The combinations of high vacuum and high temperature hot filament allow the evaporation of catalyst under a clean condition using this system. The general characterization techniques utilized to study the morphology, elemental composition and structural properties of SiNWs are briefly discussed.

3.1 PLASMA ASSISTED HOT-WIRE CHEMICAL VAPOUR DEPOSITION SYSTEM SETUP

The schematic of the home-built dual mode plasma assisted hot-wire CVD system is illustrated in Figure 3.1. The system consists of six parts, namely CVD reactor, plasma generator, hot-wire power supply, vacuum system, gas line management and heating elements.

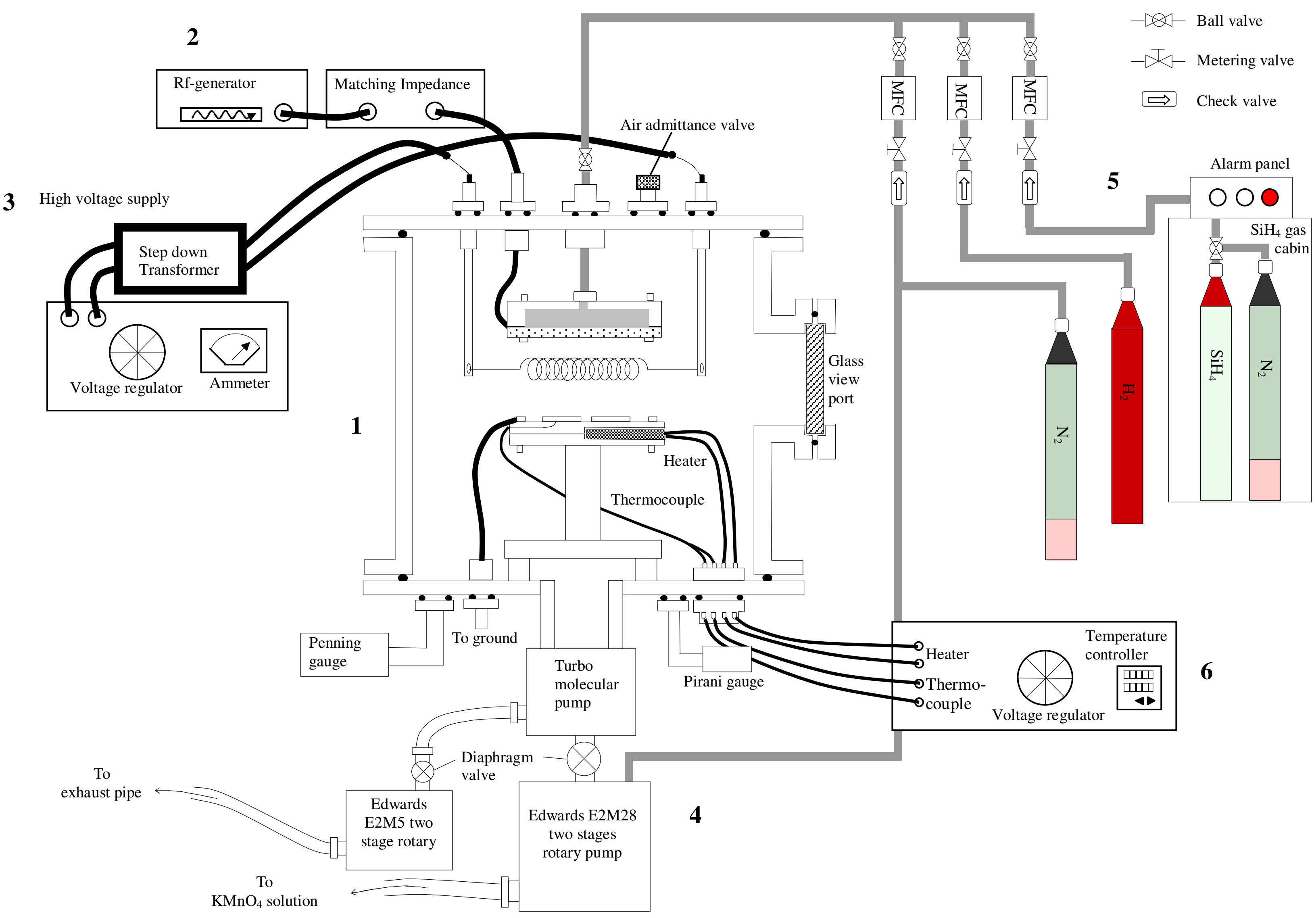

Figure 3.1: Schematic diagram of the dual modes of plasma and hot-wire assisted CVD system.

Figure 3.2: Photograph of the home-built dual modes of plasma and hot-wire assisted CVD system.

3.1.1 CVD reactor

The CVD reactor of this deposition system consists of a cylindrical stainless steel chamber with diameter of 20.5 cm and height of 48.0 cm. The CVD reactor is well-sealed with Viton o-rings and is directly connected to a vacuum pump for evacuation. The connecting tube has an air admittance valve for venting purposes. A glass viewport on the body of the reactor is used for viewing interior of the reactor. It also acts as a window for the optical pyrometer used to determine the filament temperature. A stainless steel made substrate holder is designed to hold four pieces of substrate with dimensions of 2.5 x 2.5 cm. The heater rod and thermocouple are attached to the substrate holder which is grounded to the earth and isolated from the body of the reactor by Teflon stands.

3.1.2 Plasma generator

In the CVD reactor, a stainless steel electrode-cum-gas showerhead is installed with the gas inlet tube and is placed at a distance of 5 cm from the substrate holder. The thickness and diameter of the electrode is 1 cm and 10 cm, respectively. The electrode is decorated with cone-shaped holes. The inlet and outlet diameter of the hole is 2.2 mm and 1.0 mm, respectively, while the distance between holes is 1.0 cm. Precursor gas can be dispersed uniformly from these holes. The electrode is powered for plasma generation. It is connected to the rf generator (ENI Model No: ACG-6B) via an impedance matching network. The plasma is generated between the powered electrode and grounded substrate holder by applying rf power ranging from 0 – 600 W at 13.56 MHz frequency. An impedance matching network is employed to match the load impedance of plasma to the impedance of the AC generator, so that the reflected power from plasma to rf generator can be minimized.

3.1.3 Hot-wire power supply

Tungsten wire (Good Fellow product, diameter of 0.5 mm, purity of 99.95 %) is coiled to form a solenoid shaped filament with ~30 coils of diameter 3 mm and length of ~3 cm. This filament coil serves as the hot filament for the evaporation of metal catalyst and decomposition of source gas. The tungsten filament is placed on a filament holder, which is connected to a power supply. The power supply consists of a voltage regulator (IBC voltage regulator 1P-1kVA) with voltage ranging from 0 – 250 V and a step down transformer. The transformer steps down the output voltage to a range of 0 – 20 V and maximum current of 60 A. By regulating the voltage supplied to the tungsten filament, different filament temperatures, T_f can be controlled for deposition. An ammeter is connected in series with the voltage supply to measure the current flow through the tungsten filament. T_f is measured by a pyrometer (Reytek, Raynger, 3i). The detector of the pyrometer is stimulated by the incoming infrared energy and produces a signal to the circuitry, which will process the signal and compute the T_f.

The tungsten filament is pre-heated to remove surface contaminations such as carbon and other metallic elements before deposition. Pre-heat treatment is carried out for 10 minutes at T_f ~1500°C in H_2 atmosphere with flow rate of 150 sccm.

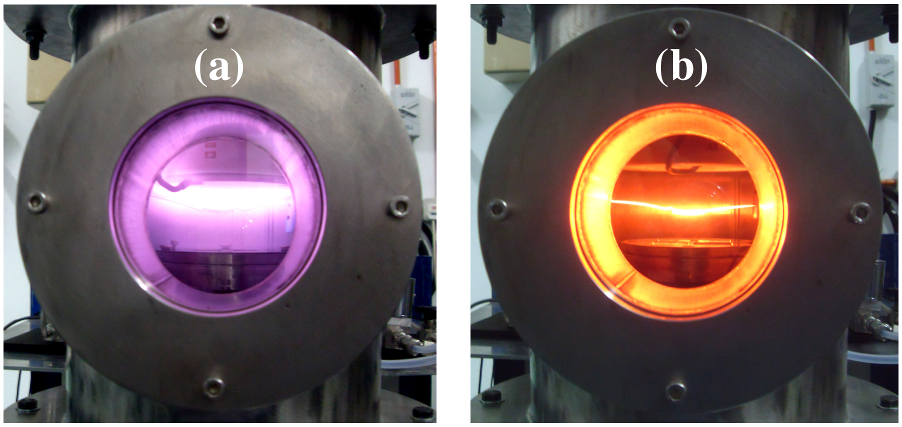

Figure 3.3: Photographs of (a) Plasma discharged silane, and (b) Hot-wire decomposed silane process.

3.1.4 Vacuum system

For the purpose of materials fabrication in CVD, a high vacuum level is important to provide a clean deposition environment and minimize contaminations in the sample. The vacuum achieved is dependent on the pump used to evacuate the system. The bottom plate of CVD reactor is directly connected to a BOC-Edwards E2M28 two-stage rotary pump and an Oerlikon Leybold Vacuum TURBOVAC TW 70H turbo molecular pump which is attached with TD 400 Turbo Drive. The E2M28 two-stage rotary pump operates at a speed of 16.2 to 19.5 ft^3min^{-1} and the ultimate vacuum achieved is ~1 x 10^{-3} mbar. It reduces the pressure of the system by repeatedly taking gas into the pump, then isolating, compressing and expelling the gas to the exhaust pipe. High vacuum pumping of the CVD system is performed by using the turbo molecular pump in conjunction with the backing of BOC-Edwards E2M5 rotary pump. It contains a rotor with inclined blades moving at high speeds of 72000 min^{-1} between the corresponding blades. Gas molecules entering the inlet port will repeatedly collide with the inclined blades, which direct these gas molecules axially downward to be removed through the backing pump. The ultimate vacuum achieved in our system is nearly 10^{-6} mbar. The vacuum levels of the CVD reactor are monitored by Pirani (Oerlikon Leybold Vacuum TTR 91) and Penning (Oerlikon Leybold Vacuum PTR 225) gauges. Pirani gauge can be operated at atmospheric to medium vacuum region (10^{3} to $5x10^{-4}$ mbar), whereas Penning gauge, also known as cold cathode gauge, is employed for high vacuum measurement (10^{-3} to 10^{-9} mbar).

3.1.5 Gas management

Highly purified SiH_4 (99.9995%) is used as the precursor gas for the synthesis of SiNWs. H_2 gas with purity of 99.999% is used to dilute the SiH_4 gas in deposition. In addition to it, H_2 gas also serves as a precursor in H_2 plasma treatment and pre-heating of coiled tungsten filament process. Purified nitrogen (N_2) gas (99.999%) is mainly used for gas line cleaning, purging and SiH_4 diluting in vacuum pump. The source gas tanks are stored in a gas room. The SiH_4 gas tank is kept in a secured gas cabinet equipped with a control panel. The source gases are introduced into the CVD reactor through the gas line, which is constructed using a 316L stainless steel tubing (outside diameter of 1/4 in). A check valve is installed in each gas line to prevent the backflow of the source gas. Ball valves are used to open or close the gas line, while metering valves are used to roughly control the amount of gas flow. The gas flow rate is accurately controlled by using a mass flow controller (MFC) with unit reading of standard cubic centimeters per minute (sccm). The SiH_4 gas flow rate is controlled by an AALBORG MFC in a flow rate range of 0 – 10 sccm. H_2 gas flow rate can be varied from 0 – 200 sccm using an Aera FC-770AC MFC with a display meter (Advanced Energy ROD-4A).

3.1.6 Heating elements

In order to prepare SiNWs samples, relatively higher substrate temperatures than film deposition are required to melt the metal catalyst or metal-Si alloy. Melting temperature for Indium is ~157^{o}C, while eutectic temperature for Au-Si alloy is ~363^{o}C at 18.6 at% of Si and 81.4 at% of Au. Hence, a basic substrate temperature of 400^{o}C is required. The heating element of the CVD system is constructed based on this temperature requirement.

A Watlow Fire Rod SFMH80 A-4183 heater cartridge is employed for substrate heating, which operates within temperature limit of <500^{o}C. The heater cartridge is clamped in between of the substrate holder, so that heat can be transferred from the stainless steel substrate holder to the substrate. The heater cartridge is connected to a voltage regulator (IBC voltage regulator 1P-1kVA) and a temperature controller (Taishio temperature controller TS-501) in a loop. The electrical power is supplied by the voltage regulator and the substrate temperature is set and controlled by the temperature controller. The temperature controller is connected to a thermocouple (Maltec-T type K thermocouple), installed at the bottom of the substrate in the CVD reactor. The thermocouple is used to directly measure the temperature of the substrate.

3.2 SUBSTRATES AND CATALYSTS

Silicon wafer serves as standard substrate for the SiNWs samples. It is suitable for most of the characterization, especially Fourier transform infrared measurement as it transmits in the infrared region. We chose a P-type Si(111) (Boron dopant) wafer manufactured by the Polishing Corporation of America, with resistivity of 0 – 10 Ohm/cm and thickness of 625 ± 25 μm as substrate.

A transparent substrate, such as glass or quartz was used to study the optical properties such as transmittance and reflectance of the SiNWs. Instead of glass, quartz substrate was used as it can be used for high temperature applications up to 1250 °C with minimized substrate effect. The Ted Pella Inc. manufactured GE124 quartz with refractive index of 1.4585 and thickness of 1 mm was used as a transparent substrate as it shows high transmittance above 92% in a wavelength range of 0.26 to 2.6 μm and has a surface flatness of ± 1 degree with 60/40 scratch/dig specifications.

ITO [$In_2O_3\,(SnO_2)_x$] coated glass, as transparent conducting substrate was also used as substrate for the deposition of SiNWs. The In_2O_3 within the ITO layer can be reduced to In element, which then allows the in-situ growth of SiNWs from the In catalyst. The ITO coated glass used is manufactured by Sigma Aldrich, with surface resistivity of 8 – 12 Ω/sq. The thickness of substrate is 1.1 mm with 150 – 300 Å of ITO layer coated.

Au wire (diameter of 0.5 mm) with purity of 99.999% manufactured by Good Fellow, and In wire (diameter of 0.5 mm) with purity of 99.999% manufactured by Kurt J. Lesker Company were employed as the source for evaporation to form metal catalyst on the substrates. The melting temperatures of Au and In are 1063°C and 157°C, respectively, which can easily be evaporated using tungsten wire.

3.3 DEPOSITION PROCESS OF SILICON NANOWIRES

Deposition process performed using the home-built dual mode plasma assisted hot-wire CVD system can be categorized into 3 steps, namely pre-deposition, deposition and post-deposition.

Table 3.1: General deposition procedures carried out for SiNWs preparation.

Pre-deposition	***Substrate cleaning***	
	System evacuation	*High vacuum*
		Empty gas line
	Substrate heating	
Deposition	***Metal catalyst evaporation***	
	Si nanowires deposition	
Post-deposition	***Gas line cleaning***	
	Chamber cleaning	

3.3.1 Substrate cleaning

Prior to the substrate cleaning, the tools such as tweezers, beakers and Petri disc were cleaned using acetone and dried under N_2 purging. The cleaning process of Si substrates followed the Radio Corporation of America (RCA)-I and II cleaning methods. (*Kern and Puotinen 1970; Kern 1993*). The solvents involved hydrochloric acid (37% HCl, M = 36.49 g/mol, diluted in H_2O_2 and deionized (DI) water in a ratio of 1:1:6), ammonia (25% NH_4OH, M = 17.03 g/mol, diluted in H_2O_2 and DI water in a ratio of 1:1:5), hydrofluoric acid (48 – 50% HF, M = 20.01 g/mol, diluted in DI water in a ratio of 1:10) and deionized (DI) water. HCl can be used to remove residual metal contaminations, such as Al, Mg and Zn. NH_4OH can be used to remove organic contaminations and dissolved metal (Au, Ag, Cu, Ni, Cd, Co and Cr) contaminations. HF is mainly used to remove native SiO_2 layer of the Si wafers.

Quartz substrates were cleaned using decon 90, acetone (C_3H_6O, M = 58.08 g/mol), ethanol (C_2H_5OH, M = 46.07 g/mol). The cleaning procedures were as proposed by Kern (*Kern 1993*). The quartz substrates were immersed in a beaker containing decon

90 solution and sonicated in ultrasonic bath for 20 minutes to remove oil and gross dirt contaminations. This was followed by rinsing in acetone, ethanol and DI water subsequently to remove organic impurities such as the hydrocarbon dried by N_2 purging.

The cleaning process of ITO coated glass is slightly different from quartz substrate as strong soap water can etch the ITO layer. Substrate cleaning procedure was carried out by rinsing the ITO coated glass in dilute ethanol solution and sonicated in ultrasonic bath for 20 minutes. It was followed by subsequently rinsing in acetone; ethanol and DI water subsequently, followed by drying. The cleaned Si, quartz and ITO coated glass substrates were placed separately in Petri dish and kept in a dry cabinet before being used in deposition.

3.3.2 System evacuation

The cleaned substrates were put onto the substrate holder and placed into the CVD reactor. The reactor was then tightly sealed. This was followed by the system evacuation. The reactor was first evacuated to a pressure below 10^{-3} mbar, then the Penning gauge was activated and the turbo molecular pump was turned on. The reactor was pumped down to a base pressure of ~2×10^{-5} mbar. Then the pressure of the reactor was kept at ~3×10^{-3} mbar. This was followed by evacuating the gas line. The valves connecting the SiH_4 and H_2 gas lines to the reactor were sequentially opened to drain out the residual gas in the gas lines. It is important to make sure that the gas lines are free from other gas contamination before introducing the source gas into the reactor for deposition.

3.3.3 Substrate heating

The substrates were heated up to a temperature of ~400^{o}C using a fire rod heater cartridge, installed at the bottom of the substrate. The substrate temperature was directly controlled by a temperature controller and the heating rate was controlled by a voltage regulator power supply. The actual value of the substrate temperature was measured using a Maltec-T type K thermocouple. When the required temperature was reached, the substrate was annealed for 15 minutes to stabilize it. This was followed by introduction of the precursor gas for deposition.

3.3.4 Metal catalyst and Si nanowires deposition

In general, the deposition involves both catalyst formation and SiNWs fabrication process. Five sets of samples were prepared and studied in this work. The deposition parameters as well as the deposition steps were altered for each set of deposition. For sets 1 and 2, the precursor gas was mainly dissociated by plasma discharge, while for sets 3, 4 and 5, hot-wire was utilized to decompose the precursor gas. The details of each deposition parameters and procedures are summarized in Table 3.3.

Table 3.2: Details of the deposition parameters for each set of samples.

No. of Set	**Technique**	**Study parameter**	**Substrate**	**H_2 plasma treatment**	**Metal evaporation**	**Deposition parameters**
1	Au evaporation using a hot-wire, followed by $SiH_4 + H_2$ gas decomposition using PECVD	Effect of substrates	p-type-c-Si(111) and ITO glass	rf power = 60 W H_2 = 150 sccm t_t = 5 minutes	l_{Au} = 2 cm Au evaporated at T_f ~1000°C in H_2 plasma treatment	P = 0.6 mbar T_s = 400°C rf power = 60 W SiH_4 = 5 sccm H_2 = 150 sccm t_d = 30 minutes
2	Simultaneous Au evaporation and $SiH_4 + H_2$ gas decomposition using HW-PECVD	Effect of rf powers	ITO glass	rf power = 60 W H_2 = 150 sccm t_t = 5 minutes	l_{Au} = 2 cm Au evaporated at T_f ~1000°C simultaneous with deposition	P = 0.6 mbar T_s = 400°C rf power = 20 – 100 W SiH_4 = 5 sccm H_2 = 150 sccm t_d = 30 minutes
3	In evaporation, followed by $SiH_4 + H_2$ gas decomposition using HWCVD	Effect of catalyst sizes	p-type-c-Si(111)	rf power = 40 W H_2 = 150 sccm t_t = 5 minutes	l_{In} = 3 – 0.5 cm In evaporated at T_f ~1200°C in H_2 plasma treatment	P = 0.7 mbar T_s = 400°C T_f = 1700°C SiH_4 = 5 sccm H_2 = 150 sccm t_d = 10 minutes

4	In evaporation, followed by $SiH_4 + H_2$ gas decomposition using HWCVD	Effect of T_f	p-type-c-Si(111)	rf power = 40 W H_2 = 150 sccm t_t = 5 minutes	l_{In} = 0.5 cm In evaporated at T_f ~1200°C in H_2 plasma treatment	P = 0.7 mbar T_s = 400 °C T_f = 1300 – 1800 °C SiH_4 = 5 sccm H_2 = 150 sccm t_d = 10 minutes
5		Effect of t_d				P = 0.7 mbar T_s = 400°C T_f = 1700°C SiH_4 = 5 sccm H_2 = 150 sccm t_d = 5 – 20 minutes

For set 1, samples were prepared by Au evaporation using heated tungsten filament followed by SiH_4 and H_2 gas decomposition using PECVD. The effect of substrates on the growth of SiNWs was studied. P-type Si(111) and ITO coated glass were used as the substrates. Au wire with purity of 99.999% (2 mm in length and 0.5 in diameter) which was tightly hung on a coiled tungsten filament was used as a source of evaporation. The Au wire was evaporated at filament temperature of ~1000^{o}C in a H_2 plasma environment with H_2 flow rate and plasma power of 150 sccm and 60 W, respectively, on the heated substrates at 400^{o}C. This was followed by the plasma decomposition of SiH_4 and H_2 gases to induce the growth of SiNWs from the catalyst. The SiH_4 and H_2 gas flow rates were maintained at 5 and 150 sccm. The substrate temperature, deposition pressure, rf power and deposition time were fixed at 400^{o}C, 0.6 mbar, 60 W and 30 min, respectively.

The deposition procedures were altered for samples preparation in set 2. SiNWs were synthesized by simultaneous Au evaporation and SiH_4 and H_2 gas decomposition using HW-PECVD. In this set of experiment, only ITO glass was used as substrate. The effect of rf power on the growth of SiNWs on ITO glass was investigated. H_2 plasma treatment was performed on the surface of heated substrate at a constant H_2 flow rate of 150 sccm for 5 minutes prior to the deposition. The coiled tungsten filament was heated to a temperature of ~1000^{o}C to evaporate the Au wire simultaneously with the dissociation of the SiH_4 and H_2 gases by rf plasma. Five samples were prepared by varying the rf power from 20 to 100 W, in an increment of 20 W. The substrate temperature, chamber pressure, SiH_4 and H_2 gases flow-rates were maintained at 400^{o}C, 0.6 mbar, 5 and 150 sccm, respectively, for each deposition. The characterization results on the as-grown SiNWs samples from sets 1 and 2 of the experiment are presented and discussed in Chapter 4.

For sets 3, 4 and 5 of the experiment, the deposition of metal catalyst and SiNWs generally followed similar deposition procedures as set 1. However, the substrate and metal wire used for deposition were replaced by p-type c-Si(111) and In wire (purity of 99.999%) with a diameter of 0.5 mm. Samples were prepared by evaporation of In followed by decomposition of SiH_4 and H_2 using HWCVD. Coiled tungsten filament with purity of 99.95% was employed as HW for In evaporation and SiH_4 and H_2 decomposition. The evaporation of In wire was carried out at T_f of about 1200^{o}C for 5 minutes under a H_2 plasma with H_2 flow rate and radio frequency power of 150 sccm and 40 W, respectively. The power of plasma generator and HW voltage supply were switched off after the evaporation. SiH_4 and H_2 gases with flow rates of 5 sccm and 150 sccm, respectively, were introduced into the chamber for the deposition, which was carried out by reheating the HW filament in order to decompose the source gases. The T_f applied during deposition was measured by a Reytek, Raynger 3i pyrometer.

For set 3 of the experiment, the effects of In catalyst size on the growth and morphology of SiNWs were studied. In catalyst size was controlled by varying the lengths of In wire being used. Three samples were synthesized by evaporation of different lengths of In wires, they were l = 3, 1 and 0.5 mm. The T_f, H_2 flow rate, SiH_4 flow rate, substrate temperature, chamber pressure and deposition time were fixed at 1700^{o}C, 150 sccm, 5 sccm, 400^{o}C, 0.7 mbar and 10 minutes, respectively, for each deposition.

For set 4 of the experiment, the effect of T_f on the growth and structural properties of SiNWs was investigated. In wire with length of 0.5 mm was used as source of evaporation in sets 4 and 5. Six samples were prepared at different T_f varying from 1300 to 1800^{o}C, with increments of 100^{o}C. The H_2 flow rate, SiH_4 flow rate, substrate temperature, chamber pressure and deposition time were fixed at 150 sccm, 5 sccm, 400°C, 0.7 mbar and 10 minutes, respectively, for all depositions.

For set 5 of the experiment, the effect of deposition time on the growth process of In-catalyzed SiNWs was studied. Three samples of SiNWs were prepared by varying the t_d at 5, 10 and 20 minutes. The deposition of SiNWs was carried out by introducing SiH_4 and H_2 gas with flow rate of 5 and 150 sccm into the reactor and the tungsten filament was heated up to a temperature of 1700°C. The substrate temperature and deposition pressure were maintained at 400°C and 0.7 mbar, respectively.

3.3.5 Post-deposition

The residual precursor gas was pumped out into the $KMnO_4OH$ solution. SiH_4 gas will react with the $KMnO_4OH$ solution to yield precipitates of MnO_4 and SiO_2. The chemical reaction equation of the process is as below:

$$3SiH_4(g) + 8KMnO_4OH(l) \rightarrow 8MnO_2(s) + 3SiO_2(s) + 8KOH(l) + 2H_2O(l) \qquad (3.1)$$

The gas line is cleaned with flowing N_2 gas to dilute the SiH_4 and avoid the precipitation of residual SiH_4 gas on the walls of the tubing. The MFC of SiH_4 gas is cleaned by N_2 purging to avoid the Si precipitation on the control valve in MFC. The system was vented when the samples were cooled down to room temperature. The samples were kept in a dry cabinet with samples characterization. The CVD reactor was cleaned for the next deposition.

3.4 CHARACTERIZATION TECHNIQUES

The characterization techniques employed to study the physical behaviors of the SiNWs involved a wide range of spectroscopy from macroscopic to microscopic level, and up to atomic level resolution; from surface (up to few nanometers from surface) to a few microns depth of sample analysis. They are categorized into 3 categories, which are morphological study, elemental composition analysis, and structural properties, according to the need of the study. The morphological study of samples is performed by field emission scanning electron microscopy. Elemental composition of the samples is examined by energy dispersion X-ray and Auger electron spectroscopes. The structural properties of samples are investigated by X-ray diffraction, micro-Raman spectroscopy and high resolution transmission electron microscopy. In the following sub-topic, the function, working principle, analytical techniques and calculations involved of each characterization techniques are briefly discussed.

3.4.1 Morphological study

3.4.1 a) Field emission scanning electron microscopy

The characterization on nanostructures is highly dependent on surface morphological imaging technique. In order to view submicron to nanosize of structures, an optical microscope is no longer applicable due to the resolution limit. Electron microscope shows much better resolution and depth of focus due to the natural behavior of electron compared to photon. Thus, SEM is commonly used to study the surface morphology of the micro/nanostructures materials.

Electron source in SEM is produced by two types of electron guns, namely thermionic and field emission guns. Field emission (FE) gun can achieve up to three orders of magnitude greater electron density, thus, higher brightness compared to the thermionic electron gun. A FE gun consists of a sharp tip (< 0.1 μm), usually made of tungsten serves as cathode and two anodes (extraction and acceleration anodes). By applying high voltage between the cathode and anodes, electron can tunnel through the energy barrier of tungsten tip into vacuum. The extraction anode (0 – 5 kV) acts to extract the electrons while the acceleration anode (1 – 50 kV) acts to accelerate the electrons by increasing the applied voltage. Electromagnetic lens are utilized to focus the electron beam by applying magnetic field in a horizontal radial direction. The scanning coil is used to deflect the electron beam to the sample by controlling the current through radially oriented coils. The incident electron beam with energy of a few hundred eV to 50 keV interacts with the sample atoms and generates a number of signals. The signals are detected and measured by a detector and transformed into a digital format of image.

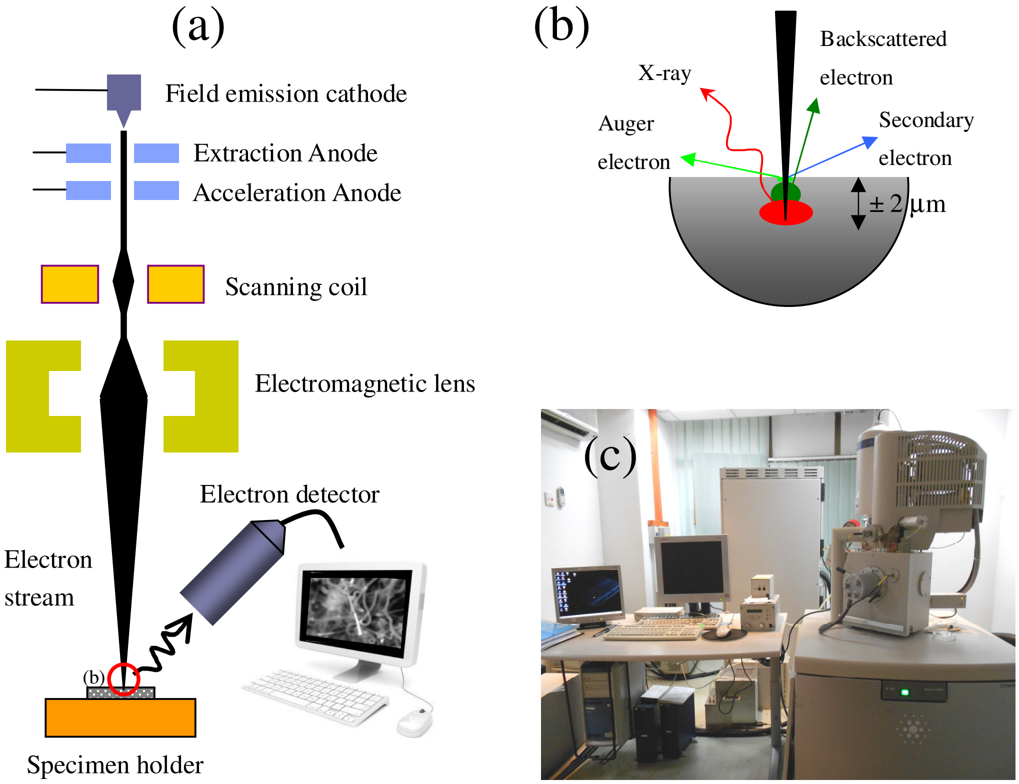

Figure 3.4: (a) schematic diagram of the main components of a FESEM, (b) schematic of the signals generated when the electron beam strikes the specimen, and (c) photograph of a FEI Quanta 200 FESEM.

Figure 3.4 (b) shows the detectable signals generated when the electron beam interacts with the sample atoms (electron or nuclei) in a FESEM. The incident electron beam collides with the electron in the sample atom bringing into an inelastic scattering and ejects the weakly bonded electron which known as secondary electron. This process is continued until the incident electron loses its energy. Typically, a single incident electron can generate > 1000 secondary electrons. This makes the secondary electron a common signal for FESEM imaging. However, secondary electron imaging mode is primarily focused in the region close to the sample surface (< 10 nm) due to its' low energy which excludes the electron extraction from deeper layer of sample. Thus, secondary electron is important in the surface topographical study of the materials.

While the incident electron collides with the nucleus in the sample atom will be elastically scattered back, which causes a detection of backscattered electron. Different from secondary electron, backscattered electron has much higher energy (few of keV) which can be utilized to identify the distribution of different elements by determining the contrast of the imaging. The intensity of the backscattered electron signal increases with the increasing of the atomic number of the elemental composition in sample. Thus, elements with higher atomic number appear brighter than the lower atomic number on the backscattered electron imaging. Both of the secondary and backscattered electrons are usually used to generate SEM image. Secondary electron gives information about the surface morphology of the sample. Backscattered electron provides information about the chemical distribution up to deeper site rather than the surface morphological study of the sample. Typical FESEM images of randomly oriented SiNWs taken by a FEI Quanta 200 FESEM using secondary electron mode are shown in Figure 3.5. The dimension of the SiNWs can be estimated from the FESEM image via the following steps. The FESEM image was printed out on an A4 paper. The scale bar of the FESEM image was equalized with the scale of a ruler (accuracy = 0.25 mm). The ruler was used to measure the dimension of the NWs. The measured values were then converted into the real values. The min and standard deviation of the real values were calculated to represent the average dimension and error bar, respectively. The number densities of the NWs were estimated from FESEM images which taken from 3 selected areas within a sample.

Meanwhile, X-ray photons and Auger electron can be emitted when the inner shell of sample atom collides with the incident electron. During the collision, the electron in the inner shell of the sample atom can be ejected from the atom, leaving an inner shell vacancy. The vacancy can be occupied by an outer shell electron and results in photon emission. The energy difference between the two shells is equivalent to the photon energy of the electromagnetic radiation in X-ray regime. Besides the X-ray radiation, another event can occur when excessive energy is transferred to another outer shell electron and this promotes the ejection of the electron from the atom shell. The ejected electron is known as Auger electron. Both the X-ray photon and Auger electron can be used for elemental analysis and the chemical composition study of the sample which will be discussed in more detail in the following section.

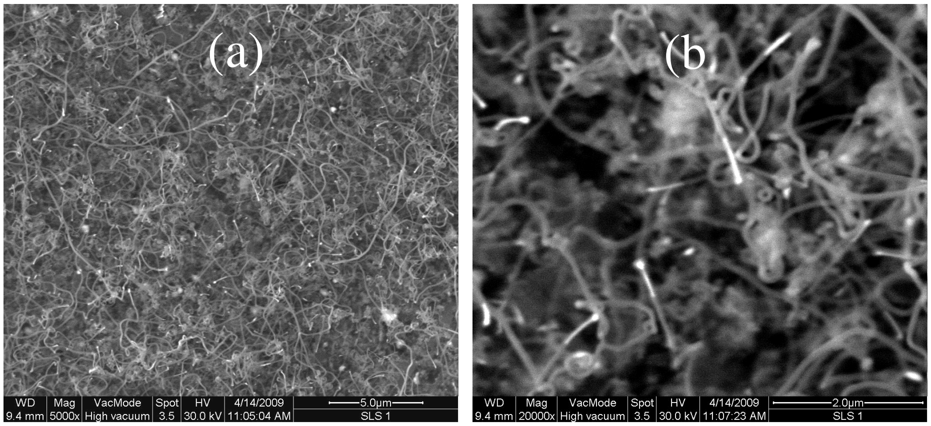

Figure 3.5: typical (a) low magnification, and (b) high magnification FESEM images of the SiNWs.

3.4.2 Elemental composition analysis

3.4.2 a) Energy dispersion X-ray

Energy-dispersion X-ray spectroscopy (EDX) provides a qualitative and quantitative analysis of the chemical composition of the SiNWs sample. The EDX detector can be attached in a SEM or TEM to effectively collect the X-ray radiation from the sample.

The radiated X-ray at all energies is collected at the same time while a complete spectrum covering the whole energy range can be acquired for analysis using EDX.

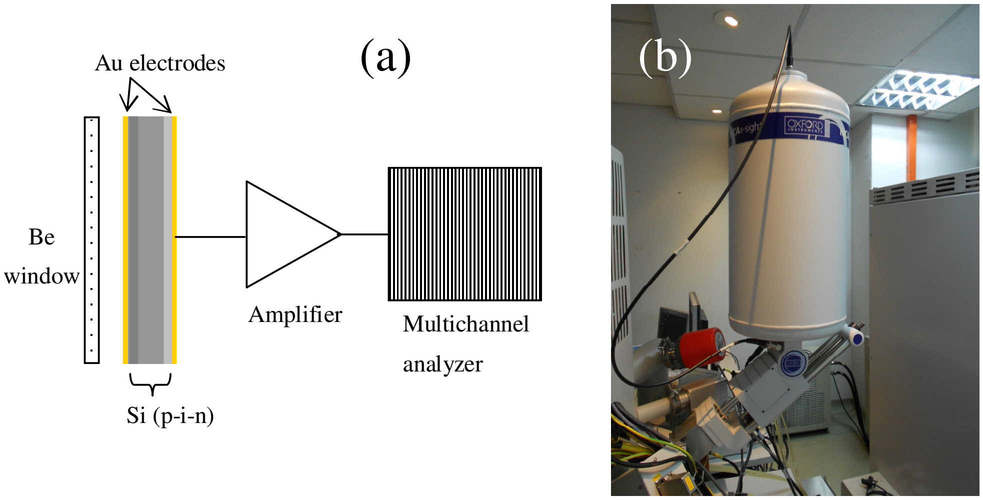

Figure 3.6: (a) A simplified schematic diagram of an EDX and (b) photograph of an INCA Energy 400 of Oxford instruments EDX attached to the FESEM.

A simplified schematic diagram of an EDX is illustrated in Figure 3.6. Generally, an EDX consists of a detector, an amplifier and a multichannel analyzer. The detector is constructed by a small piece of semiconductor plate, usually Si or germanium (Ge), with a p-i-n junction in reverse biased. The Si is doped with Li and cooled down to ~77 K with liquid N_2 to increase the resistivity of the Si plate, thus limits the current leaking through when voltage is applied through the Si plate. Both sides of the Si plate are covered by thin layers of Au electrodes (~20 nm) so that bias voltage can be applied through the p-i-n junction of Si. A thin beryllium window is placed in the outer surface of the detector to prevent contaminants coating the detector. As a result, EDX is not able to detect all elements lighter than sodium (Na) because the X-rays radiated by those light elements are not able to transmit through the beryllium window of the detector. However, utilization of Polymer-based thin windows allows for detection of light elements (C and upwards).

Incoming X-ray excites electrons into the conduction band of Si, leaving an identical number of positively charged holes in the outer shell of Si atom. The electron-hole pairs generated are directly proportional to the energy of the detected X-ray photon. When a voltage is applied across the Si plate, a current with magnitude proportional to the energy of X-ray will be generated when X-ray is absorbed into the detector. The current generated as a pulse signal when an X-ray radiation enters the detector is amplified by an amplifier and analyzed by a multichannel analyzer (MCA). The MCA acts to spread the current pulse signals into different channels according to the energy of X-rays. The EDX is controlled by a computer which also stores the energies of the X-rays from all elements. The computer is used to identify the element giving rise to a line in the spectrum or alternatively to indicate on the screen the positions on the spectrum.

In this work, the EDX measurement was carried out by an INCA Energy 400 of Oxford instruments EDX attached to the FESEM [Figure 3.6 (b)]. An example of the EDX spectra scanned on the catalyst droplet and stem of an In-catalyzed SiNW is shown in Figures 3.7 (b) and (c), respectively.

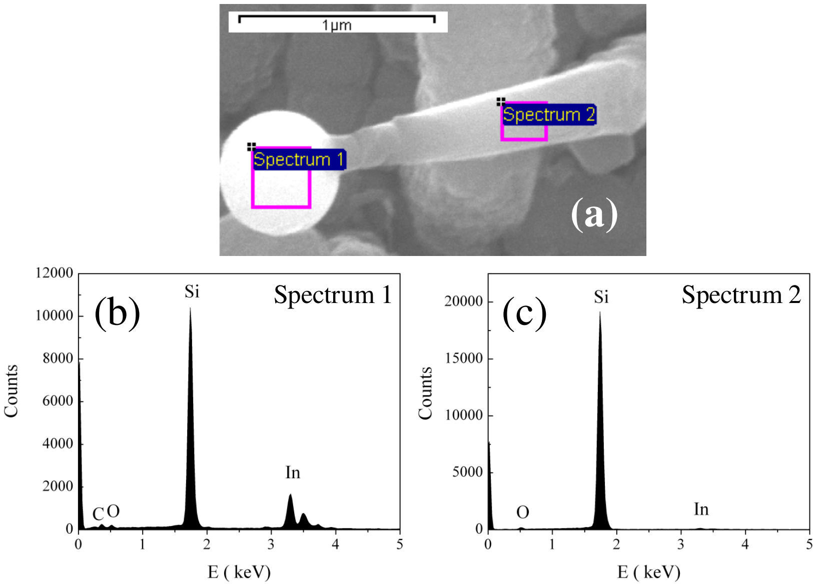

Figure 3.7: (a) FESEM image of a catalyst droplet capped SiNW. EDX spectra taken on the (b) catalyst droplet and (c) stem of the catalyst droplet capped SiNW.

3.4.2 b) Auger electron spectroscopy

Auger electron spectroscopy (AES) is developed as a surface analysis technique to study the elemental composition on the near surface (up to 5 nm depth) of material. The principle of emission of Auger electron has been discussed in the previous section. As the kinetic energy of the Auger electron is dependent on the electronic structure of the element that is unique to each atom, it can be used for identification of element in a sample. In Auger spectra, energy difference within a subshell is too small to be distinguished, thus it is usually denoted by double subscripts ($L_{2,3}$ or $M_{4,5}$).

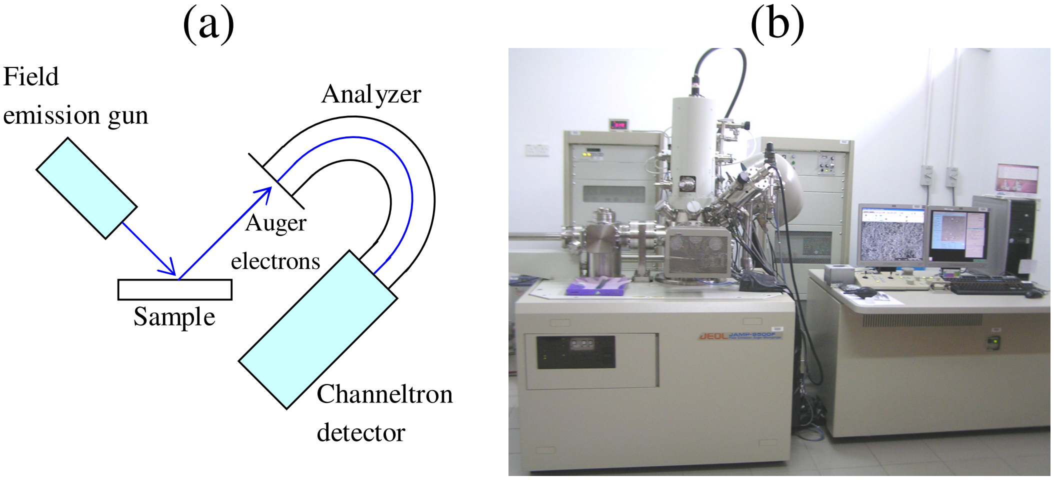

Figure 3.8: (a) Schematic diagram of an Auger electron spectroscopy and (b) photograph of a JEOL JAMP-9500F Field Emission Auger Microprobe.

Typical schematic of an AES system is shown in Figure 3.8 (a). The AES system consists of electron source, analyzer and channeltron detector. The electron beams are directed onto the sample, while the generated Auger electrons are focused onto the entrance slit of a concentric hemispherical analyzer. A potential difference is applied to the cylinders of the analyzer to deflect the detected Auger electron onto a channeltron detector. Similar to SEM, incident electron beam is generated by a field emission gun. The concentric hemispherical sector analyzer consists of a pair of hemispherical electrodes between the gaps for electron to pass through. A potential difference is applied across the electrodes with negative at outer electrode, thus electrons can be deflected by the electric field and follow the path of the mean radius in the analyzer. The Auger electron with higher energy will be deflected less while lower energy will be deflected more from the mean radius of the analyzer. The deflected Auger electron is then received by a channeltron detector. The channeltron detector is made up of a spiral-shaped glass tube with a conical collector at one end and a metal anode at the other. The output signal generated depends on the potential difference between both ends. The signal is amplified by channel electron multipliers (arrays of small multipliers) in the channeltron detector and measured by a computer in a range of energies of 0-2000 eV.

In this work, Auger electron analysis was done by a JEOL JAMP-9500F Field Emission Auger Microprobe as shown by a photograph depicted in Figure 3.8 (b). The system is equipped with a high resolution of Auger electron imaging technique, thus the Auger electron spectra for single NWs can be obtained by using a probe diameter of 8 nm. Figure 3.9 (a) shows a typical Auger electron spectrum of SiNWs prepared on ITO coated glass. The element corresponding to the Auger peaks is indexed in the figure. Differentiation of Auger electron spectrum is used to enhance the Auger signal relative to the interferences from secondary and backscattered electrons. The differential Auger electron spectrum with respect to energy, dN(E)/dE is plotted in Figure 3.9 (b), which provides a clear feature of the Auger peak, while the peak height of the derivative Auger electron spectrum is used for quantitative analysis of the element.

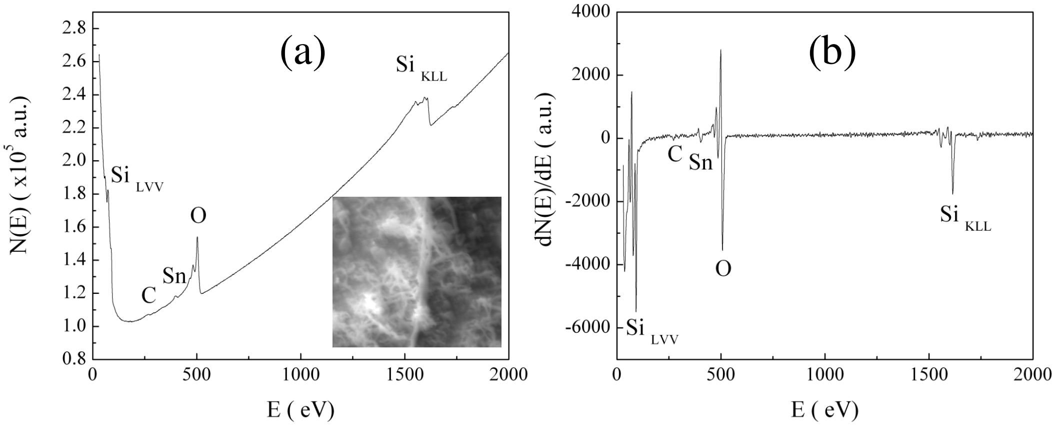

Figure 3.9: (a) Auger electron spectrum, (b) first differential Auger electron spectrum of a SiNWs sample prepared on ITO coated glass substrate.

3.4.2 c) Comparison between EDX and AES techniques

Both EDX and AES spectroscopes are powerful techniques which can be widely employed in quantitative study of elemental composition in a material. AES can detect all the elements except H, while EDX is only able to detect elements from C onwards. While, in contrast to AES, EDX has poorer detection efficiency for light element with lower atomic number, Z. Detection limit of AES and EDX is 0.1 – 1 at% (depending on the energy resolution of the elements) and 0.1 at%. The detection of any element with at% lower than the detection limit is considered as noise signal. AES has a spatial resolution of about 50 nm due to its small probe size, which has been scaled down to excellent spatial resolution of < 10 nm with finer probe size. EDX is taken under larger spot size, thus retaining wider lateral resolution of ~1 μm, which is more suitable for elemental detection within a broader area. The detection depth of AES and EDX is greatly different due to the different penetration depths of X-ray photon and Auger electron. AES is a surface analyzing technique with an effective probe depth up to ~5 nm, while EDX can obtain signal up to ~1 – 3 μm depth of a sample. The difference between the detection depth of EDX and AES can be utilized to study the elemental distribution in a sample.

Table 3.3: Analysis depth and spatial resolution of EDX and AES (*G. Cao 2004*).

Method	**Element sensitivity**	**Detection limit (at%)**	**Lateral resolution**	**Effective probe depth**
EDX	≥ C	~0.1	~1 μm	~1 – 3 μm
AES	≥ Li	~0.1 – 1	50 nm	~5 nm

3.4.3 Structural properties

3.4.3 a) X-ray diffraction

X-ray diffraction (XRD) is commonly used in characterization of the crystal structure of a material. Crystal of an element can be identified by determining the peak position in XRD pattern, while the orientation plane corresponding to the peak can be assigned. XRD provides a qualitative determination of the crystallinity of a material by analyzing the intensity of the diffraction peak. Crystallite size of the material can be quantitatively calculated from the width of the diffraction peak using several methods (*Langford et al. 1986; Patterson 1939*). As XRD is only sensitive to crystalline structures, it can be applied for both homogeneous and inhomogeneous samples, which is suitable for the structural characterization of nanomaterials.

A schematic diagram of X-ray diffractometer is illustrated in Figure 3.10 (a). The diffractometer is designed according to the Bragg-Brentano geometry. It consists of a monochromatic X-ray radiator and a detector, which are placed on the circumference of a circle centred on the sample. X-rays are generated in a cathode ray tube by accelerating electron towards a Cu anode plate. CuK_α is commonly used as X-ray source. The produced X-ray beam is then filtered by monochromator to a wavelength of 0.7 to 2 A and collimated towards sample. The X-ray beam diverges from the source and diffracted by the sample to form a convergent diffracted beam. The convergent diffracted beam is filtered by a monochromator and focused at a slit, then enters the detector. Intensity of the diffracted X-ray beam is measured as the number of current pulses per unit time by an electronic X-ray detector. During the measurement, the X-ray detector is mechanically rotated in an angle of 2θ accompanied by a rotation of sample holder in an angle of θ, while the angle of incident beam to sample holder always keeps at θ. Thus, the angle of incident beam is always equal to the angle of diffracted beam. The detector measures data of each angular increment in a minimum order of 0.01 °, while the length of time per count and step size of the angular increment are controlled by the computerized programme.

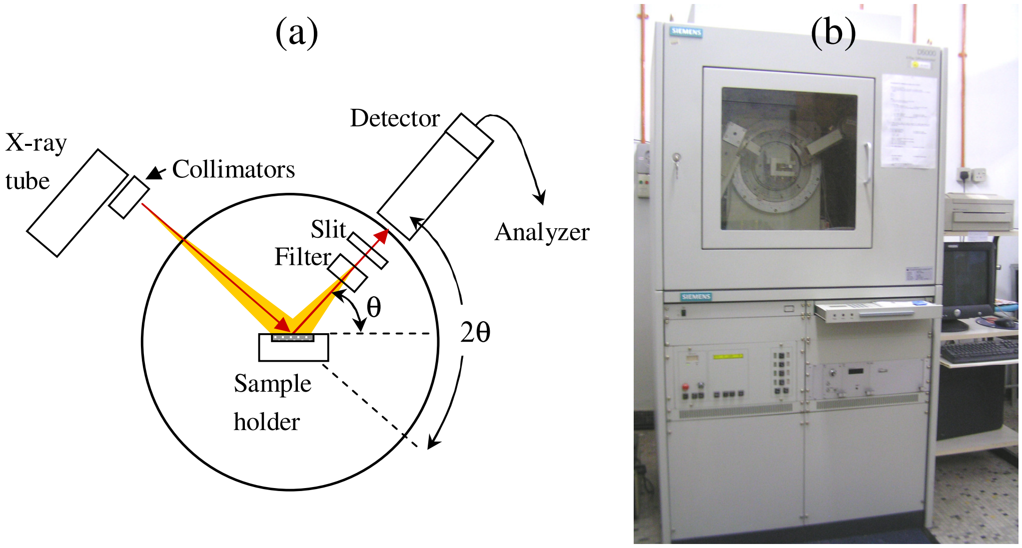

Figure 3.10: (a) schematic diagram of the X-ray diffractometer, and (b) photograph of SIEMENS D5000 X-ray diffractometer (Cu K_α X-ray radiation $\lambda = 1.5418$ Å).

When Bragg's law is satisfied in measuring a crystalline sample, the X-rays scattered by all the atoms in all of the planes are completely in phase, thereby forming constructive interference and the X-rays are diffracted at maximum intensity. This results in the diffraction peak in XRD pattern. The intensity of the diffraction peak is proportional to the degree of crystallinity of the sample. In the rest of angles, the scattered rays cancel out each other (destructive interference).

Figure 3.11 shows a typical XRD pattern of a crystalline SiNWs measured by a

SIEMENS D5000 X-ray diffractometer in a 2θ range from 10 to 80 °. The crystalline planes corresponding to the diffraction peaks of Si are indexed according to face-centered cubic Si (JCP2:00-026-1481). The dominant diffraction peak, in this case (111) orientation, is usually used for further structural analysis by deconvoluting it using Gaussian or Lorentzian function as shown in Figure 3.12. The crystallinity of SiNWs can be qualitatively evaluated by comparing the intensity and full width at half maximum (FWHM) of the Si diffraction peak with the bulk crystal Si. The crystallite size, D_x is correlated to the FWHM by Debye-Scherrer's equation as (*Patterson 1939*):

$$D_x = \frac{C\lambda}{\phi \cos\theta} \tag{3.2}$$

where λ is the wavelength of CuK_{α} (1.5418 Å), ϕ is the FWHM of the diffraction peak, θ is the angle of the diffraction peak and C is the Scherrer's constant with value of 0.89.

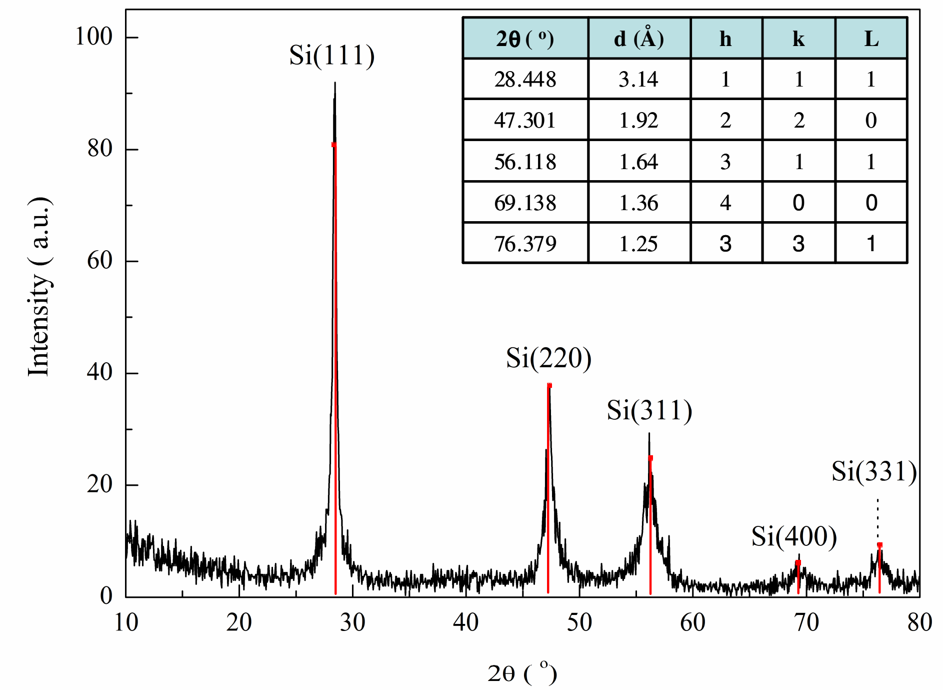

2θ (°)	d (Å)	h	k	L
28.448	3.14	1	1	1
47.301	1.92	2	2	0
56.118	1.64	3	1	1
69.138	1.36	4	0	0
76.379	1.25	3	3	1

Figure 3.11: typical XRD pattern of a crystalline SiNWs sample. Inset is a table of the lattice spacing and (hkl) orientations of each Si diffraction peak observed in the XRD pattern.

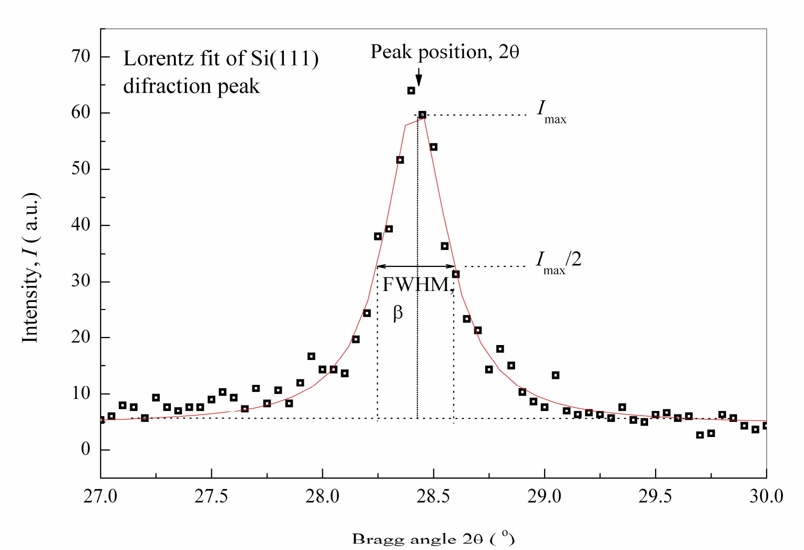

Figure 3.12: Deconvolution of the Si(111) diffraction peak using a Lorentz function.

3.4.3 b) Micro-Raman spectrometer

In addition to XRD, micro-Raman spectroscopy is used for investigating the structural properties, including crystallinity, crystalline to amorphous phase transition or vice versa, and crystalline (or amorphous) phase distribution. Basically, micro-Raman spectroscopy utilizes light scattering technique which collects the scattered light from the excitation beam through the sample. When a sample is irradiated with an intense monochromatic light source, most of the light is elastically scattered in the same wavelength as the light source by the sample. A small portion of the incident light is scattered at wavelength shifts from the excitation light source. The former is known as Rayleigh scattering, while the latter is attributed to Raman scattering. Micro-Raman spectroscopy actually measures the shift in frequency of the scattered light from the excitation light source.

Figure 3.13 (a) is a schematic of micro-Raman spectroscopy, which is constructed by a (or more than one) monochromator light sources, a video monitor and optical microscopy, a motorized stage, diffraction grating and a charge-coupled-detector (CCD). It can suit any operating range of laser source from ultraviolet to Visible and near infrared region. Laser wavelength of 632, 514, and 325 nm are typically used in micro-Raman spectroscopy for semiconducting material characterization. Argon (Ar+) and krypton (Kr+) ions lasers in numerous excitation wavelengths from 350 – 700 nm are commonly used in visible Raman measurement. For ultraviolet range, Raman measurement, yttrium aluminium garnet (YAG) laser is utilized.

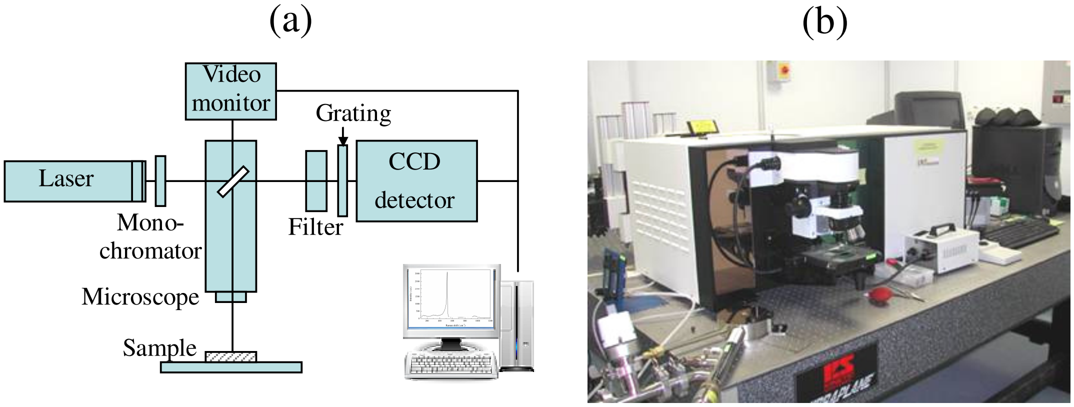

Figure 3.13: (a) schematic diagram of a micro-Raman spectrometer, and (b) photograph of a Horiba Jobin Yvon 800 UV Micro-Raman spectrometer supplied with an Ar+ laser source at an excitation wavelength of 514.5 nm.

Micro-Raman spectroscopy utilizes an optical microscope to focus the excitation laser beam onto the sample and to collect and transfer the Raman scattered light into the detector. A high magnification microscope with its smaller objective aperture can greatly improve the spatial resolution of the spectroscope to ~1 μm^2. The surface of sample can be viewed while the scanning area of the sample can be targeted by the microscope with assistance of a video monitor.

A holographic notch filter or dielectric filter is added to prevent the strong Rayleigh scattered light. Those filters will selectively reject a selected band of light, while passing the light out of the band rejection region. A grating acts to split the scattered light to its constituent wavelength and it is then collected by a CCD. The resolution of the Raman spectrum depends on the grating employed in the spectroscopy. Large grating density can eventually increase the Raman spectral resolution. The CCD is constructed by two-dimensional arrays of light sensitive elements, which are individually separated as pixels (detectors of different region or wavelength). CCD has a large wavelength response region extending from 400 to ~1000 nm, which can support laser with excitation wavelength up to 780 nm. Signals generated by the pixels are analyzed and transformed into a Raman spectrum (in wavenumber, cm^{-1} unit) by a programme in a computer.

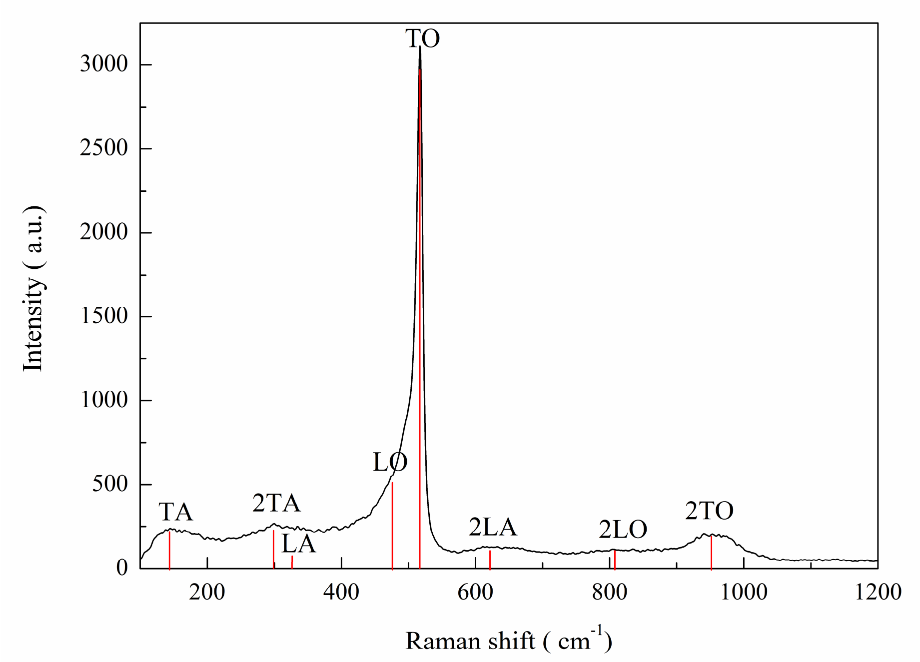

Figure 3.14: typical Raman spectrum of a crystalline SiNWs obtained from this work.

Typical Raman spectrum of crystalline SiNWs sample obtained by a Horiba Jobin Yvon 800 UV Micro-Raman spectrometer is shown in Figure 3.14. The Raman peaks correspond to the acoustic and optical vibrational modes are indexed in the spectrum. The transverse optical (TO) phonon mode of Si located at ~521 cm^{-1} is the main Raman peak of Si. The Raman intensity is given by (*Piscanec et al. 2003*):

$$I(\omega) = \int \frac{|C(0,k)|^2}{[\omega - \omega(k)]^2 + \left(\frac{\Gamma_0}{2}\right)^2} d^3k \tag{3.3}$$

where C(0,q) is a Fourier coefficient of the confinement function, k is wave vector and

Γ_0 is the FWHM of the bulk crystal Si. The Raman peak modelled by equation 3.3 generally shows a Lorentzian shape.

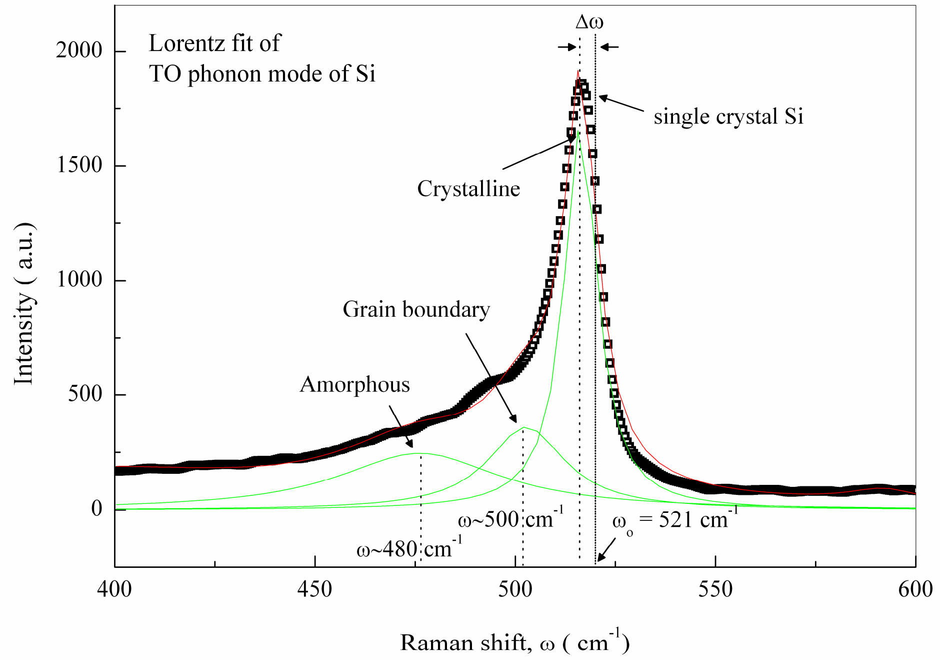

Figure 3.15: Deconvolution of the TO phonon mode of crystalline Si peak using a Lorentz function.

As described by the confinement model of Richter et al. (*Richter et al. 1981*) and Campbell and Fauchet (*Campbell and Fauchet 1986*) (RCF), the downshift and asymmetric broadening of the TO phonon mode of SiNWs is due to their confined size (with negligible localized heating by laser irradiation and internal stress in the SiNWs). According to the principle proposed in (*Shim et al. 2008*), the size of nanocrystallites, D_R can be estimated by a simplified equation such as:

$$D_R = 2\pi\sqrt{\frac{B}{\Delta\omega}} \tag{3.4}$$

where B is 2.24 $cm^{-1}nm^2$ for Si and $\Delta\omega$ is the shifting of crystalline peak from single crystal Si peak located at 521 cm^{-1}. The TO phonon mode can be deconvoluted into 3 peaks corresponding to amorphous, grain boundary or intermediate phase and crystalline components at 480 cm^{-1}, 500 cm^{-1} and 521 cm^{-1}, respectively as shown in Figure 3.15. The crystalline volume fraction, X_C of the samples can be calculated from the deconvolution data using equation as (*Mukhopadhyay et al. 2004*):

$$X_C = \frac{I_c + I_i}{\gamma I_a + I_c + I_i} \times 100\% \qquad (3.5)$$

where I_c, I_i and I_a are integrated intensities of the Raman peaks corresponding to crystalline, grain boundaries and amorphous components respectively. The factor γ is the ratio of the cross-section of the amorphous phase to the crystalline phase, and is defined as:

$$\gamma = 0.1 + \exp(-d / 250) \qquad (3.6)$$

where d is the grain size in nm. In the case of the microcrystalline and nanocrystalline Si films, with their small crystallites, γ is $\cong 1$ (*Gajović et al. 2009*). For the highly crystalline SiNWs sample, the amorphous component are absent in the TO phonon mode. Thus, the crystallinity of the sample is obtained by comparing the FWHM of the TO phonon mode with bulk crystal Si (*Nguyen et al. 2009*).

In addition, Raman mapping is one of the most powerful tools in today's micro-Raman spectroscopy to study the distribution of structures in a given area. Raman mapping image is generated from Raman spectra recorded at discrete points or lines within a selected area of the sample. It can be shown in a variation of any fitted parameter, including intensity, width and position of Raman peak as a function of the point of analysis. An example of Raman mapping image of an In-catalyzed SiNW and its optical video capturing image are shown in Figure 3.16. The video image reveals each of the probing points to acquire the Raman signals. The Raman image presents a variation of the width of the TO phonon mode of Si, where the area with higher wavelength in colour indicates higher crystallinity in structure.

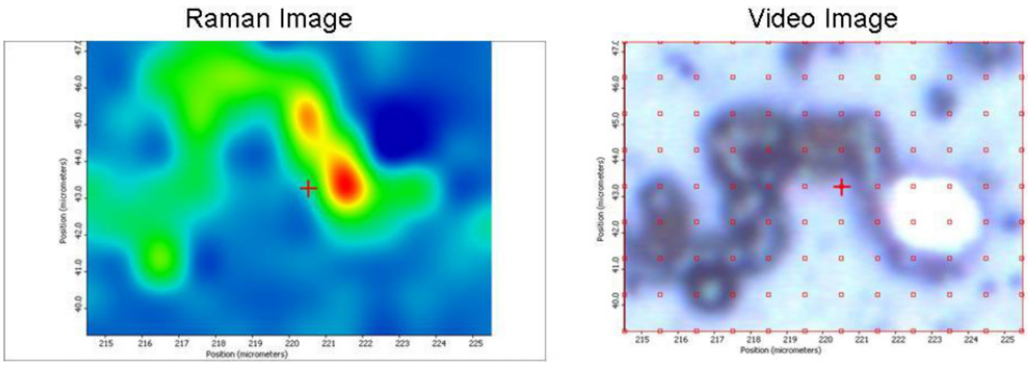

Figure 3.16: Raman image and the video capturing image of an In-catalyzed SiNWs.

3.4.3 c) High resolution transmission electron microscopy

Transmission electron microscopy (TEM) plays an important role for the characterization of the structural properties and crystallinity of the SiNWs. Atomic structure of a SiNWs can be directly investigated by employing high resolution transmission electron microscopy (HRTEM). A high resolution of ~1 Å is theoretically obtained in a HRTEM due to the shortening in de Broglie wavelength of the high energetic electron beam. This is useful in determination of the crystalline or amorphous structures and structure defects such as twinning and lattice dislocation within NWs. It can also be used to identify the atomic lattice spacing, crystalline plane, preferred orientation and growth direction of the NWs.

Figure 3.17 (a) is a schematic diagram of the main components of a TEM. Similar to SEM, TEM is constructed with an electron gun, usually field emission gun for high resolution. The voltage applied to accelerate the electron is in a range of 200 to 300 kV to allow the transmission of electron beam through the specimen. The electron beam is focused by two condenser lenses into a coherent beam, and further restricted from deviation by a condenser aperture. The focused electron beams then strike the specimen and are transmitted through the specimen. The transmitted electrons are focused by the objective lens into an image which is then passed through the intermediate and projector lenses, and then projected on the fluorescent screen. The objective and selected area apertures are used for TEM image and diffraction pattern projections, respectively. For the TEM image projection mode, the objective aperture acts to block the high angle diffracted electrons, while, for the diffraction pattern projection mode, the selected area aperture acts to assist the examination of the diffraction of electrons.

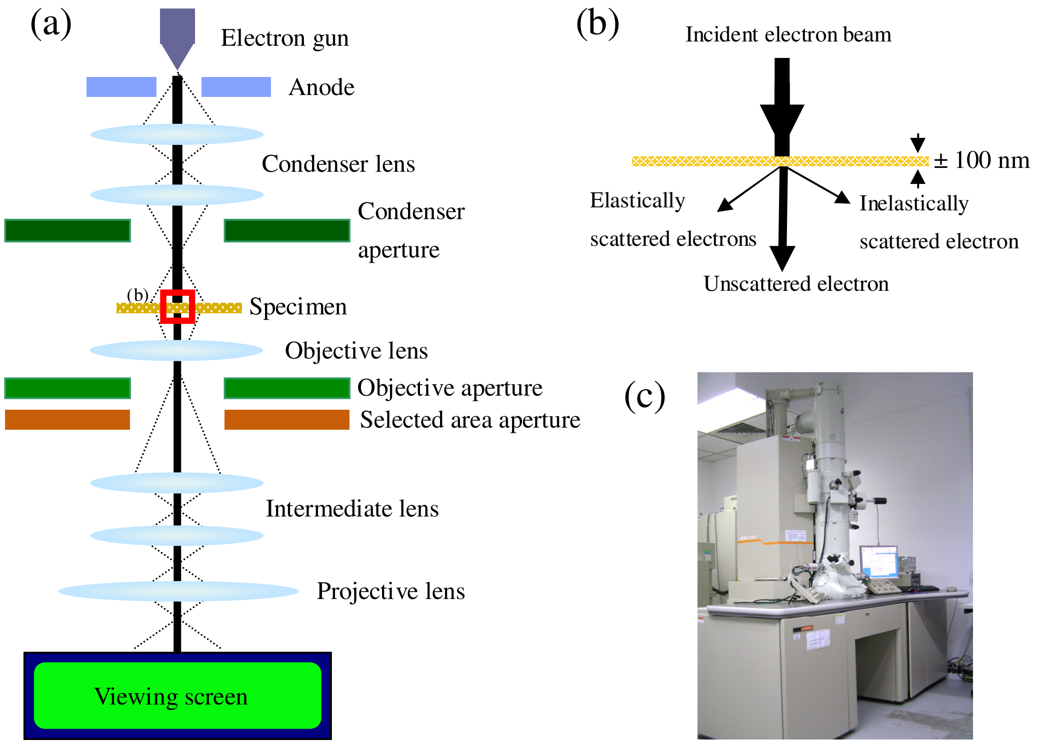

Figure 3.17: (a) schematic diagram of the main components of a HRTEM, (b) schematic of the signals generated when the electron beam strikes the specimen in the HRTEM, and (c) photograph of a JEOL JEM 3100F, 300 kV HRTEM.

The transmitted electrons can be classified into three types, namely unscattered, elastically scattered and inelastically scattered electrons. The electrons transmitted through the specimen without any interaction with the specimen atoms are called unscattered electrons. These unscattered electrons mainly contribute to the TEM images. The darker area in a TEM image can be due to the thicker or heavier element in that area, thus fewer electrons are transmitted through that area. Elastically scattered electrons are generated when the incident electrons are scattered by the specimen atoms with no loss of energy. The elastically scattered electrons follow Bragg's diffraction law, where the incident electrons are scattered by the atoms with the same atomic spacing and possess same scattering angle. The same angle of scattered electrons forms a pattern of diffraction spots. This diffraction pattern is utilized to generate selected area electron diffraction (SAED) pattern, which gives information on the structures (amorphous or crystalline), orientation and atomic arrangement of the sample. Conversely, the electrons generated when the incident electrons interact with the specimen atoms with loss in energy are inelastically scattered electrons. The inelastic loss of energy by the incident electrons is unique to each of the elements interacted with. Thus, it provides the information of the compositional and chemical bonding of the sample.

In order to obtain higher resolution (up to atomic level), the sample should be thin enough (< 100 nm) to enable the transmission of the electron beam. A TEM grid, usually copper grid with carbon supporting film, is used to hold the sample. Formvar Film 400 mesh copper grid (FF400-CU-50) is used in this work. The samples on the substrate were immersed in an ethanol solution and sonicated for about 15 minutes to extract the SiNWs from the substrate. The diluted SiNWs in an ethanol solution was then transferred onto a copper grid through a cleaned pipette. The copper grid was dried in a dry cabinet for a few hours before carrying out TEM measurement.

Figures 3.18 (a) – (c) show typical HRTEM micrographs of amorphous SiNW, single crystalline SiNW, and nanocrystalline embedded Si nanostructures, respectively, obtained by a JEOL JEM 3100F HRTEM working at voltage of 300 kV. SAED pattern of the nanocrystalline embedded Si nanostructures is shown in Figure 3.18 (d).

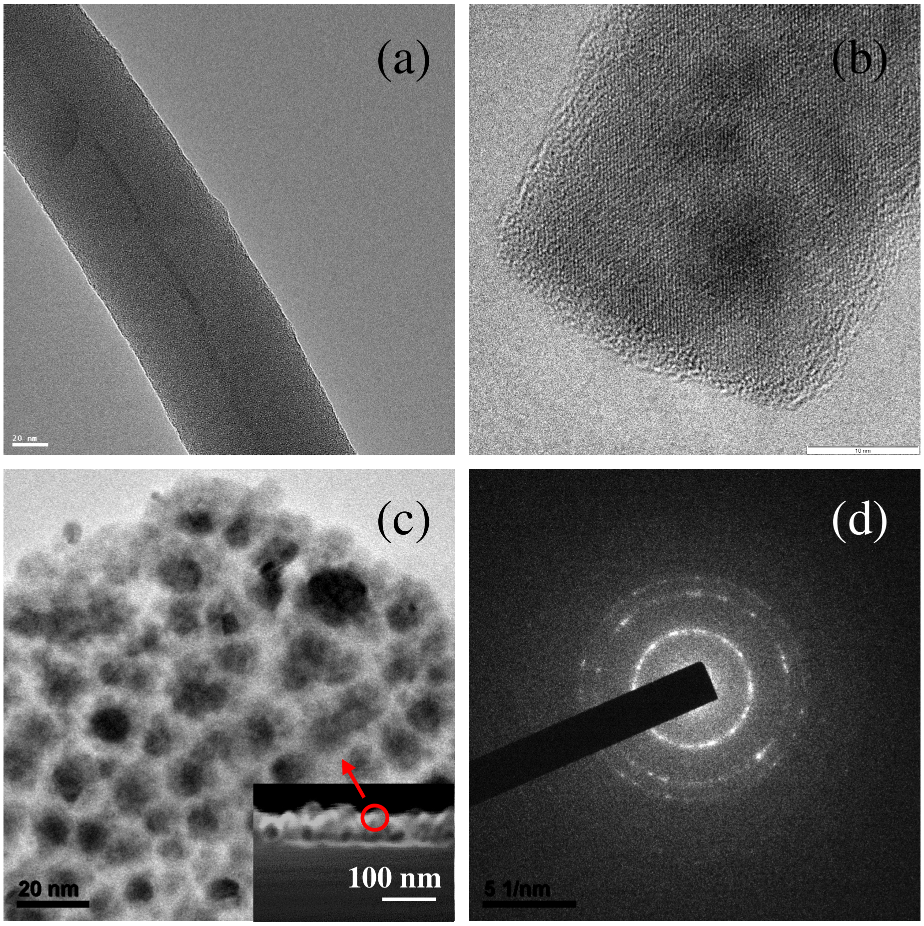

Figure 3.18: typical HRTEM micrographs of (a) amorphous SiNWs, (b) single crystalline SiNWs and (c) nanocrystalline embedded Si nanostructures produced by this work. Inset in (c) is the cross-sectional FESEM image of Si nanostructures. (d) SAED pattern of the nanocrystalline embedded Si nanostructures in (c).

3.4.3 d) Comparison between XRD, μRS and HRTEM techniques

X-ray diffractometer, micro-Raman spectroscopy and HRTEM are three different techniques, which utilize X-ray, light (UV to NIR) and electrons sources, respectively to study the structural properties of a sample. Each of the techniques shows its strengths and limitations compared to the rest. XRD is an ensemble characterization technique, where the information acquired is an average over a large amount of a material. Its minimum spot size is ~50 μm. In Bragg-Brentano geometry, the fraction of the total diffracted intensity, G_x which is contributed by a sample layer of depth, x is given as (*Cullity and Stock 2001*):

$$G_x = 1 - \exp(-2\mu x / \sin\theta) \tag{3.7}$$

where μ is the linear absorption coefficient (for Si substance and Cu K_α X-ray of λ = 1.5418 Å, μ is ~152 cm^{-1} (*Cullity and Stock 2001*)). Thus, the x in a Si sample estimated from 95% ($G_x = 0.95$) of the information on the diffraction pattern at glancing angle, $\theta = 5\,^{o}$ is ~8.6 μm. For micro-Raman spectroscopy, the lateral resolution, L, and the axial resolution, Δz, of a Si sample is depending on the wavelength of the laser light, λ and numerical aperture of the objective of Raman microscope, NA, given by (*Gouadec and Colomban 2007*):

$$L = \frac{0.61\lambda}{NA} \tag{3.8}$$

and $$\Delta z = \frac{\lambda}{(NA)^2} \tag{3.9}$$

Under the condition where λ = 514 nm and NA = 0.5, the L and Δz are about 1 and 2 μm, respectively. Therefore, XRD provides a large area structural analysis on a sample, while structural properties of selected smaller area of sample can be obtained by using micro-Raman spectroscopy. However, the high penetration depth of both techniques, especially XRD should be noted, while the measurements done on bare substrates as background were carried out before the sample analysis.

As XRD is limited in detection of amorphous structure, micro-Raman spectroscopy is more powerful in observing an amorphous to crystalline (or vice versa) transition in a Si sample. Although the reduction in size of the Si crystallites is always associated with the broadening in crystalline diffraction peak, the diffraction peak tends to be noisy with worse signal to noise ratio when the crystallite size is less than 5 nm. On the other hand, micro-Raman spectrum usually shows the suppression in crystalline component (521 cm^{-1}) accompanied by increase in the broadening of amorphous component (480 cm^{-1}), thus making it easier to monitor the short range of order structure (1 – 5 nm).

HRTEM is the best choice to study the crystallinity of a Si sample, especially SiNWs. The distribution of the crystalline and amorphous phases within the sample can be viewed from HRTEM features. Moreover, it can be used to examine the lattice dislocation and other defects in SiNWs. Intensities for electron diffraction are ~10^8 times larger than diffraction of X-ray, thus XRD generally requires large specimen and large quantity of crystalline structures to provide enough signals for the detector which however much less to construct a SAED pattern. The spatial resolution of SAED is limited to about 100 nm due to the spherical aberration of the objective lens and the size of the selected area aperture.